

MePT: Multi-Representation Guided Prompt Tuning for Vision-Language Model

Xinyang Wang¹, Yi Yang¹, Minfeng Zhu²,
Kecheng Zheng², Shi Liu¹, Wei Chen¹

¹State Key Lab of CAD&CG, Zhejiang University
²Zhejiang University

Abstract

Recent advancements in pre-trained Vision-Language Models (VLMs) have highlighted the significant potential of prompt tuning for adapting these models to a wide range of downstream tasks. However, existing prompt tuning methods typically map an image to a single representation, limiting the model’s ability to capture the diverse ways an image can be described. To address this limitation, we investigate the impact of visual prompts on the model’s generalization capability and introduce a novel method termed Multi-Representation Guided Prompt Tuning (MePT). Specifically, MePT employs a three-branch framework that focuses on diverse salient regions, uncovering the inherent knowledge within images which is crucial for robust generalization. Further, we employ efficient self-ensemble techniques to integrate these versatile image representations, allowing MePT to learn all conditional, marginal, and fine-grained distributions effectively. We validate the effectiveness of MePT through extensive experiments, demonstrating significant improvements on both base-to-novel class prediction and domain generalization tasks.

Introduction

Pre-trained vision-language models (VLMs), such as CLIP (Radford et al. 2021), have demonstrated remarkable performance across a wide range of downstream tasks in a zero-shot manner without task-specific fine-tuning. For instance, an image can be classified by using CLIP to measure the similarities with multiple textual prompts (e.g. “A photo of a {class}.”). It has been shown that the quality of text templates significantly impacts the performance of CLIP (Menon and Vondrick 2023; Radford et al. 2021). To this end, prompt tuning techniques have been developed, which not only alleviate the challenge of manually crafting prompts but also enhance the model’s generalization capabilities with minimal training data, while keeping the VLM model parameters frozen (Zhou et al. 2022b,a; Shu et al. 2022; Huang, Chu, and Wei 2022). However, a notable limitation of prompt tuning is its tendency to overfit task-specific data distributions, potentially leading to the forgetting of valuable knowledge acquired during the extensive large-scale pretraining phase (Zhou et al. 2022a).

To mitigate the issue of overfitting, existing works concentrate on reducing the discrepancy between the text

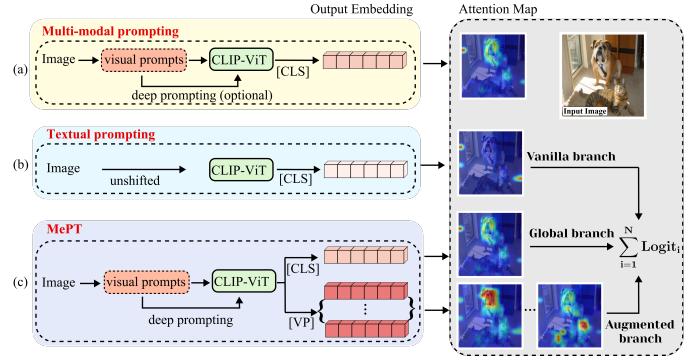


Figure 1: The illustration of multi-representation prompting. Given an image, we visualize the attention maps from the last layer of the vision transformer (Right). After visual-side prompt tuning (a), CLIP effectively optimizes the relevance signal for foreground objects compared to vanilla CLIP (b). The visual prompts (VP)s further demonstrate foreground-focused capabilities and naturally attend to different objects in the scene with diversity (c). We propose a novel Multi-Representation Guided Prompt Tuning framework, designed to capture the comprehensive information inherent in the image with three branches.

prompts and the general textual knowledge within pre-trained models. It has been approached with various strategies, including alignment with text templates (Yao, Zhang, and Xu 2023, 2024; Bulat and Tzimiropoulos 2023), integration of extra text representations (Khattak et al. 2023b; Tian et al. 2024; Zhang et al. 2024; Chen et al. 2023) and gradient-based optimization methods (Zhu et al. 2023). In addition to these approaches, visual prompt tuning technology has been introduced, to enhance synergy between the vision and language representations (Jia et al. 2022; Khattak et al. 2023a). However, existing prompt tuning techniques mainly rely on global image representations (i.e., the embedding derived from the special class token). These approaches treat the image as one single point, ignoring the fact that different text prompts may only focus on one or a subset of visual characteristics (Chen et al. 2023; Guo et al. 2023). As illustrated in Figure 1, relying solely on a global representation derived from the class token proves inade-

quate for capturing all the visual information embedded in images. This limitation constrains both the effectiveness of image recognition and the robustness of domain generalization (Chefer, Schwartz, and Wolf 2022; Paiss, Chefer, and Wolf 2022; Geirhos et al. 2020).

In efforts to incorporate more visual information, approaches such as PromptSRC (Khattak et al. 2023b) and RPO (Lee et al. 2023), despite the adoption of visual prompts, emphasize the importance of primitive image representations generated by vanilla CLIP, particularly in the category and domain shift tasks. PromptSRC aims to regulate prompted image representations by leveraging the foundational vanilla representations, while RPO utilizes multiple inner-masked visual prompts to address internal representation shifts. In contrast, our method constructs a more comprehensive representation space and leverages the synergy of diverse image representations to mitigate overfitting.

Our method employs a three-branch framework, with each branch meticulously designed to capture role-specific visual representations. The first branch termed the global branch, is pivotal as it aligns with the foundational design of the CLIP model, which is trained to match global visual features with corresponding language features. This global image representation remains indispensable for a broad range of tasks, ensuring that the foundational knowledge is retained. The second branch, referred to as the augmented branch, addresses the diverse attention patterns exhibited by learnable visual prompts. As illustrated in Figure 1, this branch utilizes outputs from visual prompts as augmented image representations, enabling a focus on different salient regions and tailoring the approach to domain-specific tasks. Additionally, these visual prompts also optimize the foreground signal for global representations, thereby improving overall model performance, with further analysis provided in our experiments. Finally, the vanilla branch is designed to preserve general visual knowledge, which is particularly beneficial for achieving generalization in unseen domains. To integrate the visual information captured by these three branches, we introduce a parameter-efficient self-ensemble strategy. Similarly to the model ensemble technique (Kang et al. 2020; Ilharco et al. 2022; Wortsman et al. 2022), the final prediction is derived from the aggregation of predictions made by each branch. This strategy enhances the model’s robustness to domain shifts and ensures comprehensive utilization of diverse visual features.

In summary, the main contributions are as follows:

- We note that the visual prompts not only enhance the model’s generalization capability but also optimize the foreground signal for global representations. Simultaneously, visual prompts themselves reveal versatile attention patterns, naturally focusing on diverse salient regions of the attention map.
- To enhance synergistic comprehension for images, we propose Multi-Representation Guided Prompt Tuning, a three-branch approach that effectively enhances robustness and generalization by ensembling global, augmented, and vanilla representations, ensuring comprehensive visual understanding.

- We conduct extensive experiments across 11 diverse datasets, collectively validating the effectiveness and robustness of our method on category shift and domain shift under few-shot generalization settings.

Related Work

Prompt Tuning in Vision-Language models

Prompt tuning, initially developed for Natural Language Processing (NLP), allows models to adapt efficiently to downstream tasks without the need to retrain previously learned parameters (Shin et al. 2020; Liu et al. 2021; Li and Liang 2021; Lester, Al-Rfou, and Constant 2021). In recent years, this technique has gained prominence in fine-tuning pre-trained VLMs, such as CLIP (Radford et al. 2021). It involves introducing learnable text and visual prompts while keeping the pre-trained weights frozen (Khattak et al. 2023a,b; Cho, Kim, and Kim 2023; Lu et al. 2022). CoOp (Zhou et al. 2022b) first introduces prompt tuning into open-world visual understanding, enabling the adaptation of knowledge from large-scale vision-language pre-trained models. Building on CoOp, its extended version, CoCoOp (Zhou et al. 2022a), enhances the generalization of learnable textual prompts for each image. To ensure that learnable text prompts retain essential general textual knowledge, approaches such as KgCoOp (Yao, Zhang, and Xu 2023), ProGrad (Zhu et al. 2023), and TCP (Yao, Zhang, and Xu 2024) have been developed. These methods constrain the prompts to align with foundational textual knowledge. Additionally, visual prompt tuning (Jia et al. 2022; Yoo et al. 2023; Oh et al. 2023) has been introduced to enhance the synergy between vision and language representations. MaPLe (Khattak et al. 2023a), RPO (Lee et al. 2023), DAPT (Cho, Kim, and Kim 2023), and promptSRC (Khattak et al. 2023b) focus on tuning both vision and language branches in order to maintain cross-modal synergy.

Visual Representation for Image Recognition

Traditionally, CLIP and prompt tuning techniques have predominantly relied on global image representations generated by a special class token (Radford et al. 2021). These tokens act as feature aggregators, providing a global summary of the input image. Recent studies (Gandelsman, Efros, and Steinhardt 2024; Darcet et al. 2024; Jia et al. 2022; Chen et al. 2023; Chowdhury et al. 2023; Sun et al. 2024) have revealed that significant potential remains for capturing and utilizing the rich information embedded within images. For instance, (Lu et al. 2024) leverages multiple pre-trained or fine-tuned VLMs to generate customized ensembles of image and text representations for decision-making. CLIP-Adapter (Gao et al. 2024) introduces an adapter mechanism to adjust visual or text embeddings, aiming to improve representation alignment. More closely related to our work, PLOT (Chen et al. 2023) extracts local visual features with varied semantic cues from feature maps. This method generates discriminative and visually-aligned local textual prompt tokens. However, PLOT has also demonstrated that depending solely on these feature maps without alignment with textual prompts can lead to a significant drop in performance.

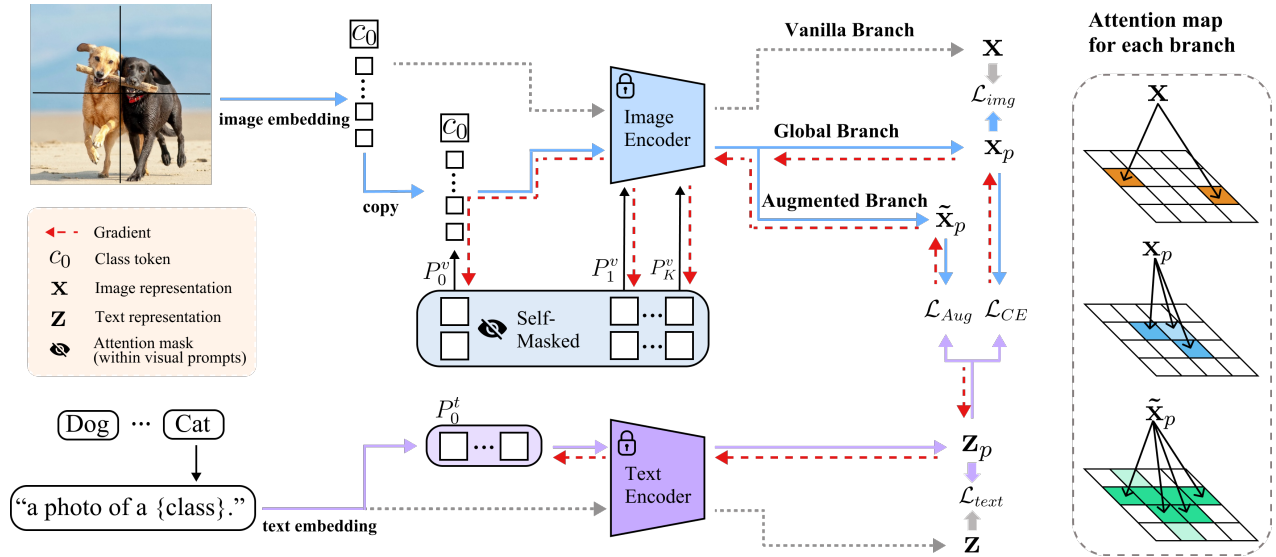


Figure 2: Overview of our proposed MePT framework for multi-modal prompt tuning. CLIP encoders are utilized to generate image and text representations from the input image-text pairs. We introduce three-branch image presentations: global representation x_p , augmented representation \tilde{x}_p , and vanilla representation x to ensure comprehensive visual understanding across different domains. Additionally, we employ ground truth supervision (\mathcal{L}_{Aug}) in the augmented branch and constraints (\mathcal{L}_{img} and \mathcal{L}_{text}) in the global branch to align with general knowledge. Moreover, the self-masked attention within visual prompts is employed to restrict the attention flow.

These studies underscore that relying solely on global representations derived from the class tokens is insufficient to capture the full range of information present in images.

Method

Preliminary

Overview. In this section, we provide an overview of the multi-modal representations in CLIP related to prompt tuning. CLIP aims to explore the semantic correspondence between the vision and language modalities through large-scale pre-training, utilizing two encoders, a transformer-based text encoder M_{text} and an image encoder M_{img} .

CLIP image and text representation. The image I and text description t are first divided into m patches and n word tokens, which are then projected into patch embeddings $E_0 \in \mathbb{R}^{m \times d_v}$ and word embeddings $W_0 \in \mathbb{R}^{n \times d_t}$. Additional special tokens, namely the *class token* c_0 and *eos token* e_0 , are included and later used as the output tokens. These embeddings E_i and W_i are inputted into the $(i+1)$ th layer of the corresponding encoder, as shown below:

$$\begin{aligned} [c_i, E_i, P_i^v] &= M_{img}^i([c_{i-1}, E_{i-1}, P_{i-1}^v]), \\ [e_i, W_i, P_i^t] &= M_{text}^i([e_{i-1}, W_{i-1}, P_{i-1}^t]) \end{aligned} \quad (1)$$

Here, $P_i^v \in \mathbb{R}^{V \times d_v}$ and $P_i^t \in \mathbb{R}^{T \times d_t}$, denote learnable prompt tokens appended after the patch and word embeddings respectively. V and T are the number of learnable visual prompts and text prompts. To obtain the final image representation x_p and text representation z_p , the output embeddings of special tokens c_K and e_K after K -layer encoders,

are projected to a common vision-language latent space:

$$x_p = \text{ImgProj}(c_K), \quad z_p = \text{TextProj}(e_K) \quad (2)$$

Prompt Tuning for CLIP. Prompt tuning, or multi-modal prompt tuning approaches, involve appending learnable prompts to either the image encoder or text encoder after original embeddings (Zhou et al. 2022b), as described in Equation (1). Each vector has the same dimension as the original word or patch embedding. For image recognition on a target dataset \mathcal{D} , learnable prompts are optimized with the cross-entropy loss \mathcal{L}_{CE} :

$$\mathcal{L}_{CE} = - \sum_{\mathcal{D}} \log \frac{\exp(\text{sim}(x_p, z_p^y)/\tau)}{\sum_{i=1}^{N_c} \exp(\text{sim}(x_p, z_p^i)/\tau)} \quad (3)$$

Here, y represents the ground truth label for the input image. By leveraging a few labeled samples, the prompts are fine-tuned specifically for the downstream task.

Multi-Representation branches

As illustrated in Figure 2, we propose a three-branch approach, with each branch dedicated to capturing role-specific visual representations. This allows MePT to learn all conditional, marginal, and fine-grained distributions effectively and uncovers the inherent knowledge within images that is essential for robust generalization.

Global branch. Since the original CLIP model is trained by aligning global visual features with language features, the global image representation is crucial for a wide range of tasks. To extend this capability, we introduce deep learnable

visual prompts $P^v = \{P_0^v, P_1^v, \dots, P_{K-1}^v\}$. For a given input sample, we obtain the final output embedding c_K by inserting learnable prompts at each layer:

$$[c_i, E_i, \tilde{P}_i^v] = M_{img}^i([c_{i-1}, E_{i-1}, P_{i-1}^v]) \quad (4)$$

Here, \tilde{P}_i^v refers to the output embedding of previous prompts P_{i-1}^v after i -th layer image encoder, while in deep prompt tuning framework, it will be replaced soon by human-introduced prompts P_i^v . The final prompted image representation is derived using the pre-trained projection matrix, as described in Equation (2), after the last vision transformer block. This output of the global branch, denoted as \mathbf{x}_p , is referred to as the *global representation*, acting as a global feature aggregator.

Augmented branch. Existing prompt-tuning methods map an image to a single global representation, which limits the model’s ability to capture the diverse ways an image can be described. To uncover the hidden knowledge of a single representation, we design the augmented branch, which enriches the image representations and exploits the foreground-focused ability of visual prompts. Specially, we obtain the final visual prompts embeddings \tilde{P}_K^v through the image encoder M_{img} , following Equation (4). These embeddings, typically discarded in previous prompt tuning methods, are then projected into the vision-language shared space to derive the corresponding representations $\tilde{\mathbf{x}}_p$:

$$\tilde{\mathbf{x}}_p = \text{ImgProj}(\tilde{P}_K^v) \quad (5)$$

We refer $\tilde{\mathbf{x}}_p$ as *augmented representation*. These representations, associated with visual prompts, are able to focus on diverse salient regions of the attention map, as shown in Figure 1, revealing excellent feature aggregation, which we will make more analysis in the next sections.

While visual prompts naturally develop the ability to focus on diverse salient regions during training, we find it beneficial to integrate a masking strategy within the visual prompts. The visual self-masked attention mechanism ensures that additional visual prompts do not interfere with each other and restricts the flow of attention to other learnable prompts (Li et al. 2023). Unlike the read-only prompts used in RPO (Lee et al. 2023), our approach with the self-masked attention module imposes no additional restrictions on image patches, thereby preserving the flow of global attention. The ablation study of the self-masked attention strategy will be provided in the next section.

Vanilla branch. Even though CLIP’s image and text encoder weights are kept frozen, learnable prompts can influence the internal representations within the self-attention module (Darcet et al. 2024; Touvron et al. 2021; Lee et al. 2023), potentially affecting performance variance and generalization, particularly in data-deficient settings. To this end, we utilize the vanilla image representation \mathbf{x} without extra learnable visual prompts appended, therefore preserving the integrity of the original features. We refer to \mathbf{x} as *vanilla representation*. This vanilla branch preserves general visual knowledge and proves to be beneficial for generalization to unseen categories and domains.

Prompt Tuning with multi-representation

Global strategy. Following the prompt tuning process, we minimize the cross-entropy loss \mathcal{L}_{CE} , as described in Equation (3). However, strong downstream dataset transfer has been shown to cause prompts to overfit task-specific data, limiting their ability to effectively utilize the general information from the frozen model (Yao, Zhang, and Xu 2023; Khattak et al. 2023b). To address this, we impose a constraint on the prompted visual and text representations to ensure their consistency with the vanilla CLIP representations by using cosine similarity:

$$\mathcal{L}_{text} = 1 - \text{sim}(\mathbf{x}_p, \mathbf{x}), \quad \mathcal{L}_{img} = 1 - \text{sim}(\mathbf{z}_p, \mathbf{z}) \quad (6)$$

In summary, we aggregate the introduced components:

$$\mathcal{L}_{Global} = \mathcal{L}_{CE} + \lambda_1 \mathcal{L}_{text} + \lambda_2 \mathcal{L}_{img} \quad (7)$$

The \mathcal{L}_{Global} loss guides the global branch to acquire complementary knowledge from both the downstream tasks and the pre-trained CLIP model, with λ_1 and λ_2 as the corresponding hyperparameters.

Augmented strategy. Visual prompts, as previously discussed, exhibit versatile attention patterns that enable them to focus on various objects within a scene. Following Equation (5), by introducing V individual visual prompt tokens, we obtain augmented representations $\tilde{\mathbf{x}}_p = \{\tilde{\mathbf{x}}_p^1, \tilde{\mathbf{x}}_p^2, \dots, \tilde{\mathbf{x}}_p^V\}$. These representations are then used to calculate similarity scores with the corresponding text representations. The final logits are obtained by averaging the similarity scores with the equal weight:

$$\text{sim}(\tilde{\mathbf{x}}_p, \mathbf{z}_p) = \frac{1}{V} \sum_{i=1}^V \frac{\tilde{\mathbf{x}}_p^i \cdot \mathbf{z}_p}{\|\tilde{\mathbf{x}}_p^i\| \|\mathbf{z}_p\|} \quad (8)$$

Although the augmented branch is designed to capture diverse salient regions, it requires additional supervision to fully leverage its potential for downstream image recognition tasks, particularly when starting from random initialization (Wang et al. 2024). To harness the full potential of these visual prompts, we propose an augmented strategy tailored specifically for domain-specific image representations:

$$\mathcal{L}_{Aug} = - \sum_{\mathcal{D}} \log \frac{\exp(\text{sim}(\tilde{\mathbf{x}}_p, \mathbf{z}_p^y)/\tau)}{\sum_{i=1}^{N_c} \exp(\text{sim}(\tilde{\mathbf{x}}_p, \mathbf{z}_p^i)/\tau)} \quad (9)$$

Here, we incorporate classification supervision using ground truth labels to enhance the branch’s few-shot visual recognition. N_c is the number of seen classes. Consequently, our overall training objective is defined as:

$$\mathcal{L} = \mathcal{L}_{Global} + \mathcal{L}_{Aug} \quad (10)$$

Representations with self-ensemble. Unlike methods that map an image to a single representation, our MePT method proposes a three-branch framework for fine-grained comprehension of each image. We employ a parameter-efficient self-ensemble strategy that integrates global image representation \mathbf{x}_p , domain-augmented representation $\tilde{\mathbf{x}}_p$, and primitive image representation \mathbf{x} to enhance robustness to domain shifts. By computing the similarity between

each image representation and the corresponding text representations, we derived predictions for each branch: $p(y|\mathbf{x}_p)$, $p(y|\tilde{\mathbf{x}}_p)$, $p(y|\mathbf{x})$. These outputs are then combined using our logit-level self-ensemble strategy, yielding the final classification results. Notably, unlike the traditional ensemble technique (Kang et al. 2020; Lu et al. 2024), our self-ensemble strategy is implemented within a single-phase prompt tuning process and does not require a secondary model for conditioning. A comparative analysis of various ensemble strategies, such as confidence weighting (Lu et al. 2024) and thresholding method (Bai et al. 2024), will be discussed in our ablation experiments.

Experiment

Benchmark Setting

Base-to-novel class generalization. We assess the generalizability of MePT by adopting a benchmark setting where the datasets are divided into base and novel classes, as outlined in (Zhou et al. 2022a). The model is initially trained solely on the base classes in a few-shot setting and is then evaluated on both the base and novel classes to measure its ability to generalize across different categories.

Cross-dataset generalization. To assess the robustness of our approach in transferring to unseen datasets, we directly evaluate our ImageNet-trained model on a variety of previously unseen datasets, without performing any data-specific fine-tuning. This allows us to validate the model’s ability to generalize effectively across different domains.

Quantitative segmentation. We follow a standard protocol for evaluating heatmap-based methods (Chefer, Gur, and Wolf 2021a,b) to validate the proposed method. In this process, the raw attention map is considered a foreground segmentation of the image and is compared against the ground truth segmentation of the dataset. The performance of the method is quantitatively assessed using three key metrics: (i) pixel accuracy (pixAcc), (ii) mean Intersection over Union (mIoU), and (iii) mean Average Precision (mAP).

Datasets. To evaluate our method’s generalization capability from base to novel classes and its performance across diverse datasets, we conduct experiments on 11 image recognition datasets: ImageNet (Deng et al. 2009), Caltech101 (Fei-Fei, Fergus, and Perona 2004), OxfordPets (Parkhi et al. 2012), StanfordCars (Krause et al. 2013), Flowers102 (Nilsback and Zisserman 2008), Food101 (Bossard, Guillaumin, and Van Gool 2014), FGVC Aircraft (Maji et al. 2013), SUN397 (Xiao et al. 2010), DTD (Cimpoi et al. 2014), EuroSAT (Helber et al. 2019), and UCF101 (Soomro, Zamir, and Shah 2012). To ensure a fair comparison, we adhere to the protocol established by CoCoOp (Zhou et al. 2022a), randomly sampling 16 images per class for the training set. Each experiment is repeated three times with different random seeds, and the average performance is reported. Additionally, we assess segmentation quality on ImageNet-Segmentation (Guillaumin, Küttel, and Ferrari 2014), a subset of the ImageNet validation set comprising 4,276 images with annotated segmentations.

Dataset		CoOp	CoCoOp	RPO	MaPLe	Prompt-SRC	MePT (Ours)
Average	Base	82.69	80.47	81.13	82.28	84.26	84.63
	Novel	63.22	71.69	75.00	75.14	76.10	76.30
	HM	71.66	75.83	77.78	78.55	79.97	80.25
ImageNet	Base	76.47	75.98	76.60	76.66	77.60	77.96
	Novel	67.88	70.43	71.57	70.54	70.73	69.88
	HM	71.92	73.10	74.00	73.47	74.01	73.70
Caltech101	Base	98.00	97.96	97.97	97.74	98.10	98.47
	Novel	89.81	93.81	94.37	94.36	94.03	94.39
	HM	93.73	95.84	96.03	96.02	96.02	96.39
OxfordPets	Base	93.67	95.20	94.63	95.43	95.33	96.09
	Novel	95.29	97.69	97.50	97.76	97.30	97.45
	HM	94.47	96.43	96.05	96.58	96.30	96.77
Cars	Base	78.12	70.49	73.87	72.94	78.27	79.93
	Novel	60.40	73.59	75.53	74.00	74.97	73.54
	HM	68.13	72.01	74.69	73.47	76.58	76.60
Flowers	Base	97.60	94.87	94.13	95.92	98.07	97.94
	Novel	59.67	71.75	76.67	72.46	76.50	76.15
	HM	74.06	81.71	84.50	82.56	85.95	85.68
Food101	Base	88.33	90.70	90.33	90.71	90.67	90.58
	Novel	82.26	91.29	90.83	92.05	91.53	91.41
	HM	85.19	90.99	90.58	91.38	91.10	90.99
Aircraft	Base	40.44	33.41	37.33	37.44	42.73	43.74
	Novel	22.30	23.71	34.20	35.61	37.87	36.79
	HM	28.75	27.74	35.70	36.50	40.15	39.97
SUN397	Base	80.60	79.74	80.60	80.82	82.67	82.53
	Novel	65.89	76.86	77.80	78.70	78.47	77.43
	HM	72.51	78.27	79.18	79.75	80.52	79.90
DTD	Base	79.44	77.01	76.70	80.36	83.37	82.64
	Novel	41.18	56.00	62.13	59.18	62.97	66.22
	HM	54.24	64.85	68.61	68.16	71.75	73.52
EuroSAT	Base	92.19	87.49	86.63	94.07	92.90	94.00
	Novel	54.74	60.04	68.97	73.23	73.90	76.85
	HM	68.69	71.21	76.79	82.35	82.32	84.56
UCF101	Base	84.69	82.33	83.67	83.00	87.10	87.04
	Novel	56.05	73.45	75.43	78.66	78.80	79.14
	HM	67.46	77.64	79.34	80.77	82.74	82.90

Table 1: Comparison with state-of-the-art methods on base-to-novel class prediction. HM represents the harmonic mean of the test accuracy on base and novel classes.

Implementation details. In all experiments, we employ a pre-trained CLIP model with a ViT-B/16 vision encoder backbone (Dosovitskiy et al. 2021) as our foundational architecture. For the base-to-novel class generalization setting, we employ deep visual and text prompt tuning, with prompts initialized randomly using a normal distribution. The learning rate is fixed at 0.0016, with a batch size of 32, and training is conducted over 50 epochs. We assign $\lambda_1 = 3$ and $\lambda_2 = 4$ to appropriately weight the text loss \mathcal{L}_{text} and image loss \mathcal{L}_{img} , respectively. The length of the text prompts, T , is set to 4, while the length of the visual prompts, V , is set to 32. For cross-dataset generalization, we set the visual prompt length V to 8, with the learning rate fixed at 0.05 and the number of training epochs at 10. In the segmentation evaluation, to more clearly demonstrate the impact of visual prompts on image representation, we exclusively employ deep visual prompt tuning (Jia et al. 2022) without incorporating additional modules. Refer to the Appendix for additional implementation details.

	Source		Target									
	ImageNet	Caltech101	OxfordPets	Cars	Flowers	Food101	Aircraft	SUN397	DTD	EuroSAT	UCF101	Average
CLIP	66.72	92.94	89.07	65.29	71.30	86.11	24.87	62.62	44.56	47.69	66.77	65.12
CoOp	71.51	93.70	89.14	64.51	68.71	85.30	18.47	64.15	41.92	46.39	66.55	63.88
CoCoOp	71.02	94.43	90.14	65.32	71.88	86.06	22.94	67.36	45.73	45.37	68.21	65.74
PromptSRC	71.27	93.60	90.25	65.70	70.25	86.15	23.90	67.10	46.87	45.50	68.75	65.81
MePT	72.09	93.54	90.71	65.47	70.93	85.81	23.57	67.70	45.61	48.38	69.38	66.11

Table 2: Comparison of MePT with existing advanced approaches on cross-dataset benchmark evaluation.

Method	Base Acc.	Novel Acc.	HM
Independent V-L prompting (IVLP)	83.65	70.64	76.60
1: Vanilla branch	77.65	75.30	76.46
2: Augmented branch	<u>83.88</u>	71.23	<u>77.04</u>
3: Global branch	84.03	<u>75.17</u>	79.35

Table 3: Effect of our proposed three-branch framework. Results are presented for each individual branch. Underlined values indicate sub-optimal performance.

Base-to-Novel Generalization

We compare the performance of our approach with CoOp (Zhou et al. 2022b), CoCoOp (Zhou et al. 2022a), RPO (Lee et al. 2023), MaPLe (Khattak et al. 2023a), and PromptSRC (Khattak et al. 2023b). Table 1 provides a comparative analysis of our methods against these baseline models for base and novel class prediction, demonstrating that MePT consistently outperforms previous methods. Specifically, MePT significantly enhances performance over CoCoOp by 4.16% for base classes and 4.61% for novel classes, and over the deep multi-modal prompt tuning method MaPLe by 2.35% and 1.16%, respectively. We attribute these improvements to the integration of both vanilla and augmented representations, which effectively bridge the distributional gap between the downstream tasks and the pretraining dataset, thereby enhancing performance. Notably, on datasets with a larger distributional gap from ImageNet (Khattak et al. 2023a), such as EuroSAT (a satellite imagery dataset) and DTD (a texture dataset), MePT demonstrates substantial improvements. For instance, MePT achieves a 13% performance gain over CoCoOp on the EuroSAT dataset. The overall trend suggests that MePT’s effectiveness increases with the diversity of the dataset. However, it is important to note that we do not employ class-specific context or text-side augmentation, which results in lower performance on fine-grained classification datasets. For instance, both CoOp and MePT, without text-side augmentation, underperform compared to PromptSRC on the Flower dataset.

Cross-Dataset Evaluation

We evaluate the cross-dataset generalization capability of MePT by training multi-modal prompts on all 1000 ImageNet classes and then directly applying them to the remaining 10 datasets. Table 2 presents the cross-dataset evaluation results, comparing our method with state-of-the-art

Method	Base Acc.	Novel Acc.	HM
1: Global	84.03	75.17	79.35
2: Global + Vanilla	83.30	<u>76.04</u>	79.50
3: Global + Vanilla + Augment	<u>84.57</u>	75.86	<u>79.98</u>
4: Global + Promitive + maskAugment	84.63	76.30	80.25

Table 4: Effect of our proposed multi-representation techniques. Results are averaged over 11 datasets.

Method	Base Acc.	Novel Acc.	HM
1: Confidence weighting	84.04	76.30	79.98
2: Threshold (>0.8)	84.55	76.18	80.15
3: Equal weighting (mean)	84.63	76.30	80.25

Table 5: Comparison of branch ensemble strategies. Equal-weighted branch ensemble strategy demonstrates superior performance over others.

approaches. Overall, our tuning method exhibits the best generalization performance across the target datasets while maintaining robust classification capabilities on the ImageNet source dataset. Compared to CoOp, our approach shows competitive results and achieves superior generalization on 9 out of 10 datasets.

Segmentation Results

As shown in Figure 3, with the evaluation of attention-based explainability methods, we analyze the raw attention map outputs of the images from both the class token and visual prompts. These outputs are binarized to generate foreground/background segmentation maps. By comparing the segmentation quality with the zero-shot results produced by the vanilla CLIP, we observe that, after few-shot visual prompts tuning, the segmentation accuracy consistently surpassed that of zero-shot methods across all metrics. The improvements are closely correlated with the number of visual prompt tokens utilized, suggesting that visual prompt tuning effectively optimizes the relevance signal for foreground objects while reducing the model’s reliance on irrelevant background cues. Further, the visual prompts exhibit foreground representational capabilities that are comparable to, and in some cases exceed, those of the special class token. These visual prompts naturally attend to diverse objects of the attention map, even when initialized randomly.

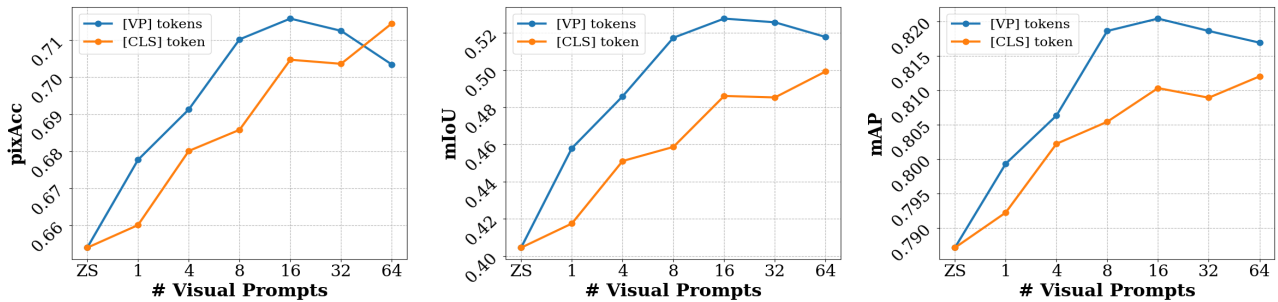


Figure 3: Comparison of foreground/background segmentation results of the special class token ([CLS]) and visual prompts tokens ([VP]s) with zero-shot CLIP baseline. The visual prompts are trained on ImageNet with 16-shot per base class.

Ablation Experiments

Effectiveness of three-branch presentations. We employ a simple baseline method, Independent Vision-Language Prompting (IVLP) (Khattak et al. 2023a), which learns deep prompt tokens separately on both the text and image encoders. To evaluate the individual contributions of our multi-representation branches, we disentangle them within our prompting framework, as shown in Table 3 and Table 4. Incorporating the vanilla branch results in a significant 4.66% increase in novel class performance, although it leads to a 6.00% decrease in base class performance. This indicates that the vanilla branch effectively enforces prompts to capture generalizable features from the frozen CLIP model, yet struggles with domain-specific tasks. For the augmented branch, performance improvements are observed in both base and novel classes, with gains of 0.23% and 0.59%, respectively. Additionally, in this branch, both base class and novel class performance surpass the IVLP baseline, achieving near-optimal results. This suggests that, with ground truth supervision, the visual prompts are capable of effectively classifying and recognizing both in-domain and out-of-domain distributions. As for the global branch, it leads to significant performance gains, with base class accuracy increasing by 0.39% and a substantial improvement of 4.53% in novel class accuracy.

Moreover, as illustrated in Table 4, by ensembling these role-specific branches, we note that the vanilla branch substantially enhances performance on unseen categories, while the self-masked augmented branch predominantly improves performance on seen categories.

Comparison on ensemble strategies. Table 5 presents a comparative study of different prompt ensemble techniques. We evaluate our approach against two baseline methods. The first baseline utilizes a confidence-aware weighting ensemble (Lu et al. 2024; Liu et al. 2023), which adjusts the logits of different branches according to their respective confidence levels. The second baseline utilizes a logit level thresholding method (Bai et al. 2024; Feng et al. 2021), applying a threshold of 0.8 to the outputs of the three branches. In contrast, our equal weighting aggregation strategy achieves the highest average performance across both base and novel classes across 11 datasets.

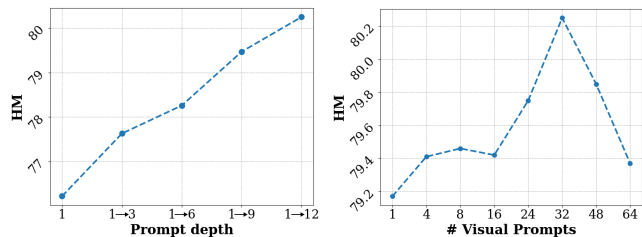


Figure 4: Ablation study on prompt depth (left) and visual prompt length (right) over 11 datasets.

Prompt depth. Figure 4 (left) illustrates the impact of prompt depth on performance. Generally, performance improves as the prompt depth increases. This trend is consistent with findings reported by (Jia et al. 2022; Yoo et al. 2023), where employing deep vision-language prompts across all layers yields the highest harmonic mean.

Prompt length. Figure 4 (right) presents the effect of visual prompt length on the harmonic mean. Overall, performance initially improves as the prompt length increases, but after reaching an optimal point, it begins to decline. Specifically, the highest harmonic mean is achieved with a prompt length of 32 vision prompts.

Conclusion

In this paper, we propose Multi-Representation Guided Prompt Tuning (MePT), a novel approach designed to enhance robustness and generalization in vision-language models. Our method employs a three-branch strategy that ensembles global, augmented, and vanilla image representations, thereby providing a synergistic and comprehensive understanding of visual information across a wide range of domains. The experimental results demonstrate that our approach significantly improves performance on image recognition tasks across various datasets, validating its effectiveness and robustness. Our method provides a direction for enriching image representations through visual prompts, but further research is needed to fully explore the impact of these visual prompts and the underlying mechanisms through which they affect the overall image representation.

References

- Bai, S.; Zhang, M.; Zhou, W.; Huang, S.; Luan, Z.; Wang, D.; and Chen, B. 2024. Prompt-based distribution alignment for unsupervised domain adaptation. In *Proceedings of the AAAI Conference on Artificial Intelligence*, volume 38, 729–737.
- Bossard, L.; Guillaumin, M.; and Van Gool, L. 2014. Food-101—mining discriminative components with random forests. In *European Conference on Computer Vision*, 446–461.
- Bulat, A.; and Tzimiropoulos, G. 2023. Lasp: Text-to-text optimization for language-aware soft prompting of vision & language models. In *Proceedings of the IEEE/CVF Conference on Computer Vision and Pattern Recognition*, 23232–23241.
- Chefer, H.; Gur, S.; and Wolf, L. 2021a. Generic attention-model explainability for interpreting bi-modal and encoder-decoder transformers. In *Proceedings of the IEEE/CVF International Conference on Computer Vision*, 397–406.
- Chefer, H.; Gur, S.; and Wolf, L. 2021b. Transformer interpretability beyond attention visualization. In *Proceedings of the IEEE/CVF conference on computer vision and pattern recognition*, 782–791.
- Chefer, H.; Schwartz, I.; and Wolf, L. 2022. Optimizing relevance maps of vision transformers improves robustness. *Advances in Neural Information Processing Systems*, 35: 33618–33632.
- Chen, G.; Yao, W.; Song, X.; Li, X.; Rao, Y.; and Zhang, K. 2023. PLOT: Prompt Learning with Optimal Transport for Vision-Language Models. In *The Eleventh International Conference on Learning Representations*.
- Cho, E.; Kim, J.; and Kim, H. J. 2023. Distribution-aware prompt tuning for vision-language models. In *Proceedings of the IEEE/CVF International Conference on Computer Vision*, 22004–22013.
- Chowdhury, M. N. R.; Zhang, S.; Wang, M.; Liu, S.; and Chen, P.-Y. 2023. Patch-level routing in mixture-of-experts is provably sample-efficient for convolutional neural networks. In *International Conference on Machine Learning*, 6074–6114. PMLR.
- Cimpoi, M.; Maji, S.; Kokkinos, I.; Mohamed, S.; and Vedaldi, A. 2014. Describing textures in the wild. In *Proceedings of the IEEE conference on computer vision and pattern recognition*, 3606–3613.
- Darcet, T.; Oquab, M.; Mairal, J.; and Bojanowski, P. 2024. Vision Transformers Need Registers. In *The Twelfth International Conference on Learning Representations*.
- Deng, J.; Dong, W.; Socher, R.; Li, L.-J.; Li, K.; and Fei-Fei, L. 2009. Imagenet: A large-scale hierarchical image database. In *2009 IEEE conference on computer vision and pattern recognition*, 248–255. Ieee.
- Dosovitskiy, A.; Beyer, L.; Kolesnikov, A.; Weissenborn, D.; Zhai, X.; Unterthiner, T.; Dehghani, M.; Minderer, M.; Heigold, G.; Gelly, S.; Uszkoreit, J.; and Houshy, N. 2021. An Image is Worth 16x16 Words: Transformers for Image Recognition at Scale. In *International Conference on Learning Representations*.
- Fei-Fei, L.; Fergus, R.; and Perona, P. 2004. Learning generative visual models from few training examples: An incremental bayesian approach tested on 101 object categories. In *2004 conference on computer vision and pattern recognition workshop*, 178–178. IEEE.
- Feng, H.; You, Z.; Chen, M.; Zhang, T.; Zhu, M.; Wu, F.; Wu, C.; and Chen, W. 2021. KD3A: Unsupervised Multi-Source Decentralized Domain Adaptation via Knowledge Distillation. In Meila, M.; and Zhang, T., eds., *Proceedings of the 38th International Conference on Machine Learning*, volume 139 of *Proceedings of Machine Learning Research*, 3274–3283. PMLR.
- Gandelsman, Y.; Efros, A. A.; and Steinhardt, J. 2024. Interpreting CLIP’s Image Representation via Text-Based Decomposition. In *The Twelfth International Conference on Learning Representations*.
- Gao, P.; Geng, S.; Zhang, R.; Ma, T.; Fang, R.; Zhang, Y.; Li, H.; and Qiao, Y. 2024. Clip-adapter: Better vision-language models with feature adapters. *International Journal of Computer Vision*, 132(2): 581–595.
- Geirhos, R.; Jacobsen, J.-H.; Michaelis, C.; Zemel, R.; Brendel, W.; Bethge, M.; and Wichmann, F. A. 2020. Shortcut learning in deep neural networks. *Nature Machine Intelligence*, 2(11): 665–673.
- Guillaumin, M.; Küttel, D.; and Ferrari, V. 2014. Imagenet auto-annotation with segmentation propagation. *International Journal of Computer Vision*, 110: 328–348.
- Guo, Z.; Zhang, R.; Qiu, L.; Ma, X.; Miao, X.; He, X.; and Cui, B. 2023. Calip: Zero-shot enhancement of clip with parameter-free attention. In *Proceedings of the AAAI Conference on Artificial Intelligence*, volume 37, 746–754.
- Helber, P.; Bischke, B.; Dengel, A.; and Borth, D. 2019. Eurosat: A novel dataset and deep learning benchmark for land use and land cover classification. *IEEE Journal of Selected Topics in Applied Earth Observations and Remote Sensing*, 12(7): 2217–2226.
- Hendrycks, D.; Basart, S.; Mu, N.; Kadavath, S.; Wang, F.; Dorundo, E.; Desai, R.; Zhu, T.; Parajuli, S.; Guo, M.; et al. 2021a. The many faces of robustness: A critical analysis of out-of-distribution generalization. In *Proceedings of the IEEE/CVF international conference on computer vision*, 8340–8349.
- Hendrycks, D.; Zhao, K.; Basart, S.; Steinhardt, J.; and Song, D. 2021b. Natural adversarial examples. In *Proceedings of the IEEE/CVF conference on computer vision and pattern recognition*, 15262–15271.
- Huang, T.; Chu, J.; and Wei, F. 2022. Unsupervised prompt learning for vision-language models. *arXiv preprint arXiv:2204.03649*.
- Ilharco, G.; Wortsman, M.; Gadre, S. Y.; Song, S.; Hajishirzi, H.; Kornblith, S.; Farhadi, A.; and Schmidt, L. 2022. Patching open-vocabulary models by interpolating weights. *Advances in Neural Information Processing Systems*, 35: 29262–29277.
- Jia, M.; Tang, L.; Chen, B.-C.; Cardie, C.; Belongie, S.; Hariharan, B.; and Lim, S.-N. 2022. Visual prompt tun-

- ing. In *European Conference on Computer Vision*, 709–727. Springer.
- Kang, T.; Chen, P.; Quackenbush, J.; and Ding, W. 2020. A novel deep learning model by stacking conditional restricted boltzmann machine and deep neural network. In *Proceedings of the 26th ACM SIGKDD international conference on knowledge discovery & data mining*, 1316–1324.
- Khattak, M. U.; Rasheed, H.; Maaz, M.; Khan, S.; and Khan, F. S. 2023a. Maple: Multi-modal prompt learning. In *Proceedings of the IEEE/CVF Conference on Computer Vision and Pattern Recognition*, 19113–19122.
- Khattak, M. U.; Wasim, S. T.; Naseer, M.; Khan, S.; Yang, M.-H.; and Khan, F. S. 2023b. Self-regulating prompts: Foundational model adaptation without forgetting. In *Proceedings of the IEEE/CVF International Conference on Computer Vision*, 15190–15200.
- Krause, J.; Stark, M.; Deng, J.; and Fei-Fei, L. 2013. 3d object representations for fine-grained categorization. In *Proceedings of the IEEE international conference on computer vision workshops*, 554–561.
- Lee, D.; Song, S.; Suh, J.; Choi, J.; Lee, S.; and Kim, H. J. 2023. Read-only prompt optimization for vision-language few-shot learning. In *Proceedings of the IEEE/CVF International Conference on Computer Vision*, 1401–1411.
- Lester, B.; Al-Rfou, R.; and Constant, N. 2021. The power of scale for parameter-efficient prompt tuning. In *Conference on Empirical Methods in Natural Language Processing*.
- Li, J.; Li, D.; Savarese, S.; and Hoi, S. 2023. Blip-2: Bootstrapping language-image pre-training with frozen image encoders and large language models. In *International conference on machine learning*, 19730–19742. PMLR.
- Li, X. L.; and Liang, P. 2021. Prefix-tuning: Optimizing continuous prompts for generation. In *Proceedings of the 59th Annual Meeting of the Association for Computational Linguistics and the 11th International Joint Conference on Natural Language Processing*.
- Liu, X.; Ji, K.; Fu, Y.; Du, Z.; Yang, Z.; and Tang, J. 2021. P-tuning v2: Prompt tuning can be comparable to fine-tuning universally across scales and tasks. In *Proceedings of the 59th Annual Meeting of the Association for Computational Linguistics and the 11th International Joint Conference on Natural Language Processing*.
- Liu, Y.; Zhang, J.; Chen, Q.; and Peng, Y. 2023. Confidence-aware Pseudo-label Learning for Weakly Supervised Visual Grounding. In *Proceedings of the IEEE/CVF International Conference on Computer Vision (ICCV)*, 2828–2838.
- Lu, Y.; Liu, J.; Zhang, Y.; Liu, Y.; and Tian, X. 2022. Prompt distribution learning. In *Proceedings of the IEEE/CVF Conference on Computer Vision and Pattern Recognition*, 5206–5215.
- Lu, Z.; Bai, J.; Li, X.; Xiao, Z.; and Wang, X. 2024. Beyond Sole Strength: Customized Ensembles for Generalized Vision-Language Models. In *Forty-first International Conference on Machine Learning*.
- Maji, S.; Rahtu, E.; Kannala, J.; Blaschko, M.; and Vedaldi, A. 2013. Fine-grained visual classification of aircraft. *arXiv preprint arXiv:1306.5151*.
- Menon, S.; and Vondrick, C. 2023. Visual Classification via Description from Large Language Models. In *The Eleventh International Conference on Learning Representations*.
- Nilsback, M.-E.; and Zisserman, A. 2008. Automated flower classification over a large number of classes. In *2008 Sixth Indian conference on computer vision, graphics & image processing*, 722–729. IEEE.
- Oh, C.; Hwang, H.; Lee, H.-y.; Lim, Y.; Jung, G.; Jung, J.; Choi, H.; and Song, K. 2023. Blackvip: Black-box visual prompting for robust transfer learning. In *Proceedings of the IEEE/CVF Conference on Computer Vision and Pattern Recognition*, 24224–24235.
- Paiss, R.; Chefer, H.; and Wolf, L. 2022. No token left behind: Explainability-aided image classification and generation. In *European Conference on Computer Vision*, 334–350. Springer.
- Parkhi, O. M.; Vedaldi, A.; Zisserman, A.; and Jawahar, C. 2012. Cats and dogs. In *2012 IEEE conference on computer vision and pattern recognition*, 3498–3505. IEEE.
- Radford, A.; Kim, J. W.; Hallacy, C.; Ramesh, A.; Goh, G.; Agarwal, S.; Sastry, G.; Askell, A.; Mishkin, P.; Clark, J.; et al. 2021. Learning transferable visual models from natural language supervision. In *International conference on machine learning*, 8748–8763. PMLR.
- Recht, B.; Roelofs, R.; Schmidt, L.; and Shankar, V. 2019. Do imagenet classifiers generalize to imagenet? In *International conference on machine learning*, 5389–5400. PMLR.
- Selvaraju, R. R.; Cogswell, M.; Das, A.; Vedantam, R.; Parikh, D.; and Batra, D. 2017. Grad-cam: Visual explanations from deep networks via gradient-based localization. In *Proceedings of the IEEE international conference on computer vision*, 618–626.
- Shin, T.; Razeghi, Y.; IV, R. L. L.; Wallace, E.; and Singh, S. 2020. AutoPrompt: Eliciting Knowledge from Language Models with Automatically Generated Prompts. In *Empirical Methods in Natural Language Processing*.
- Shu, M.; Nie, W.; Huang, D.-A.; Yu, Z.; Goldstein, T.; Anandkumar, A.; and Xiao, C. 2022. Test-time prompt tuning for zero-shot generalization in vision-language models. *Advances in Neural Information Processing Systems*, 35: 14274–14289.
- Soomro, K.; Zamir, A. R.; and Shah, M. 2012. A dataset of 101 human action classes from videos in the wild. *Center for Research in Computer Vision*, 2(11): 1–7.
- Sun, Z.; Fang, Y.; Wu, T.; Zhang, P.; Zang, Y.; Kong, S.; Xiong, Y.; Lin, D.; and Wang, J. 2024. Alpha-clip: A clip model focusing on wherever you want. In *Proceedings of the IEEE/CVF Conference on Computer Vision and Pattern Recognition*, 13019–13029.
- Tian, X.; Zou, S.; Yang, Z.; and Zhang, J. 2024. ArGue: Attribute-Guided Prompt Tuning for Vision-Language Models. In *Proceedings of the IEEE/CVF Conference on Computer Vision and Pattern Recognition*, 28578–28587.

Touvron, H.; Cord, M.; Douze, M.; Massa, F.; Sablayrolles, A.; and Jégou, H. 2021. Training data-efficient image transformers & distillation through attention. In *International conference on machine learning*, 10347–10357. PMLR.

Wang, H.; Ge, S.; Lipton, Z.; and Xing, E. P. 2019. Learning robust global representations by penalizing local predictive power. *Advances in Neural Information Processing Systems*, 32.

Wang, Y.; Cheng, L.; Fang, C.; Zhang, D.; Duan, M.; and Wang, M. 2024. Revisiting the Power of Prompt for Visual Tuning. In *Forty-first International Conference on Machine Learning*.

Wortsman, M.; Ilharco, G.; Kim, J. W.; Li, M.; Kornblith, S.; Roelofs, R.; Lopes, R. G.; Hajishirzi, H.; Farhadi, A.; Namkoong, H.; et al. 2022. Robust fine-tuning of zero-shot models. In *Proceedings of the IEEE/CVF conference on computer vision and pattern recognition*, 7959–7971.

Xiao, J.; Hays, J.; Ehinger, K. A.; Oliva, A.; and Torralba, A. 2010. Sun database: Large-scale scene recognition from abbey to zoo. In *2010 IEEE computer society conference on computer vision and pattern recognition*, 3485–3492. IEEE.

Yao, H.; Zhang, R.; and Xu, C. 2023. Visual-language prompt tuning with knowledge-guided context optimization. In *Proceedings of the IEEE/CVF conference on computer vision and pattern recognition*, 6757–6767.

Yao, H.; Zhang, R.; and Xu, C. 2024. TCP: Textual-based Class-aware Prompt tuning for Visual-Language Model. In *Proceedings of the IEEE/CVF Conference on Computer Vision and Pattern Recognition*, 23438–23448.

Yoo, S.; Kim, E.; Jung, D.; Lee, J.; and Yoon, S. 2023. Improving visual prompt tuning for self-supervised vision transformers. In *International Conference on Machine Learning*, 40075–40092. PMLR.

Zhang, Y.; Zhang, C.; Yu, K.; Tang, Y.; and He, Z. 2024. Concept-Guided Prompt Learning for Generalization in Vision-Language Models. In *Proceedings of the AAAI Conference on Artificial Intelligence*, volume 38, 7377–7386.

Zhou, K.; Yang, J.; Loy, C. C.; and Liu, Z. 2022a. Conditional prompt learning for vision-language models. In *Proceedings of the IEEE/CVF conference on computer vision and pattern recognition*, 16816–16825.

Zhou, K.; Yang, J.; Loy, C. C.; and Liu, Z. 2022b. Learning to prompt for vision-language models. *International Journal of Computer Vision*, 130(9): 2337–2348.

Zhu, B.; Niu, Y.; Han, Y.; Wu, Y.; and Zhang, H. 2023. Prompt-aligned gradient for prompt tuning. In *Proceedings of the IEEE/CVF International Conference on Computer Vision*, 15659–15669.

Supplementary Material

The supplementary material contents are organized in the following order:

- Additional implementation details (Appendix A)
- Domain generalization experiments (Appendix B)
- GradCAM segmentation results (Appendix C)
- Additional loss ablation study (Appendix D)
- Qualitative results of attention map (Appendix E)

A. Additional implementation details

Additional training details. In all experiments, we employ a pre-trained CLIP model with a ViT-B/16 vision encoder backbone (Dosovitskiy et al. 2021). All models are trained using the SGD optimizer and utilize NVIDIA RTX 4090D GPU. In segmentation evaluation experiments, to more clearly demonstrate the impact of visual prompts on image representation, we exclusively employ deep visual prompt tuning (Jia et al. 2022) without incorporating additional modules, and the learning rate is fixed at 0.002. We train on base ImageNet (Deng et al. 2009) classes with 16-shot to be consistent with the base-to-novel experiments.

Domain generalization settings. Additionally, we evaluate the robustness of our method on out-of-distribution datasets. The domain generalization capability of MePT is assessed by training multi-modal prompts on all 1000 ImageNet classes and then directly applying them to four other ImageNet variants that contain various types of domain shifts. The four ImageNet variants include ImageNetV2 (Recht et al. 2019), ImageNet-Sketch (Wang et al. 2019), ImageNet-A (Hendrycks et al. 2021b) and ImageNet-R (Hendrycks et al. 2021a). In these domain generalization experiments, all hyperparameters are kept the same as in the cross-dataset settings. We employ deep visual and text prompt tuning, with prompts initialized randomly using a normal distribution. The learning rate is fixed at 0.05, with a batch size of 32, and training is conducted over 10 epochs. We assign $\lambda_1 = 3$ and $\lambda_2 = 4$ to appropriately weight the text loss \mathcal{L}_{text} and image loss \mathcal{L}_{img} , respectively. The visual prompt length V is set to 8 and the text prompt length T is set to 4.

B. Domain generalization

Table 6 presents the domain generalization results, comparing our method with state-of-the-art approaches. Overall, our tuning method exhibits favorable generalization performance across the four ImageNet variants while maintaining robust classification capabilities on the ImageNet source dataset. Specifically, MePT significantly improves performance on ImageNetV2 by 0.92% compared to the previous state-of-the-art method, promptSRC. Compared to CoCoOp and MaPLe, our approach achieves superior generalization on 3 out of 4 datasets and shows excellent overall results.

C. GradCAM segmentation results

We also evaluate segmentation performance with GradCAM (Selvaraju et al. 2017). GradCAM is a class-specific visualization technique that combines the input features with the

	Source		Target			
	ImageNet	-V2	-S	-A	-R	Avg.
CLIP	66.73	60.83	46.15	47.77	73.96	57.18
CoOp	71.51	64.20	47.99	49.71	75.21	59.28
CoCoOp	71.02	64.07	48.75	50.63	76.18	59.91
MaPLe	70.72	64.07	49.15	50.90	76.98	60.27
PromptSRC	71.27	64.35	49.55	50.90	77.80	60.65
MePT	72.09	65.27	49.39	49.56	77.21	60.36

Table 6: Comparison of MePT with existing advanced approaches on domain generalization benchmark evaluation.

gradients of the network’s final layer to highlight salient regions in the input image. The GradCAM segmentation evaluation settings are identical to those used for the raw attention map analysis mentioned earlier. For GradCAM, we use the textual category that obtains the highest similarity score with the image to compute the gradient that is propagated. As illustrated in Figure 5, with few-shot visual prompt tuning and using the output embeddings derived from the special class token ([CLS]), both the class-agnostic behavior of the raw attention map and the class-specific behavior of GradCAM demonstrate significant improvement in highlighting foreground objects.

D. Additional loss ablation study

Table 7 presents ablation studies of losses employed in the MePT framework, namely \mathcal{L}_{Aug} , \mathcal{L}_{img} and \mathcal{L}_{text} . The loss \mathcal{L}_{Aug} provides additional supervision, fully leveraging the potential of visual prompts for downstream image recognition tasks and domain-specific image representation. The ablation study shows that removing \mathcal{L}_{Aug} results in a significant performance drop of 2.46% on base classes, with only a minimal impact on novel classes, causing the 0.13% drop. This indicates that \mathcal{L}_{Aug} is crucial to improve performance on base classes. Conversely, \mathcal{L}_{img} and \mathcal{L}_{text} are employed to constrain the prompted visual and text representations, ensuring consistency with the vanilla CLIP representation. The ablation experiment results show that removing \mathcal{L}_{img} and \mathcal{L}_{text} leads to a continuous performance drop of 2.93% on novel classes, while there is a performance gain of 0.61% on base classes. This suggests that \mathcal{L}_{img} and \mathcal{L}_{text} are crucial for maintaining performance on novel classes, but their presence may limit the model’s ability to effectively recognize images in seen classes.

Method	Base Acc.	Novel Acc.	HM
w/o $\mathcal{L}_{Aug}, \mathcal{L}_{text}, \mathcal{L}_{img}$	82.78	73.24	77.72
w/o \mathcal{L}_{Aug}	82.17	76.17	79.06
MePT	84.63	76.30	80.25

Table 7: Effect of losses employed in MePT framework.

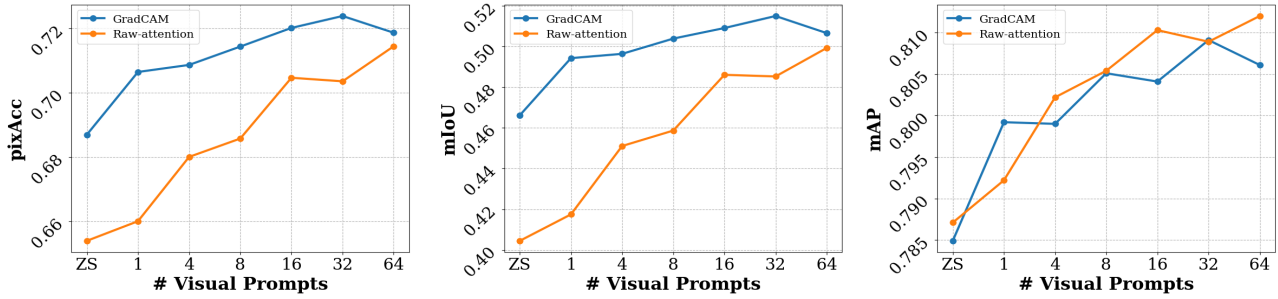


Figure 5: Comparison of foreground/background segmentation results between the GradCAM and raw attention map using the output embeddings derived from the special class token ([CLS]), relative to the zero-shot CLIP baseline. The visual prompts are trained on ImageNet with 16-shot per base class.

E. Qualitative results of attention map

In Figure 6, we visualize the attention maps from the last layer of the Vision Transformer, using visual prompts trained on ImageNet with 16 shots per category. Our approach generates diverse attention maps that highlight more salient regions on foreground objects while reducing reliance on irrelevant background cues. This enhanced focus on foreground areas explains the observed improvements in downstream image recognition tasks, particularly in category and domain shift scenarios under few-shot generalization settings.

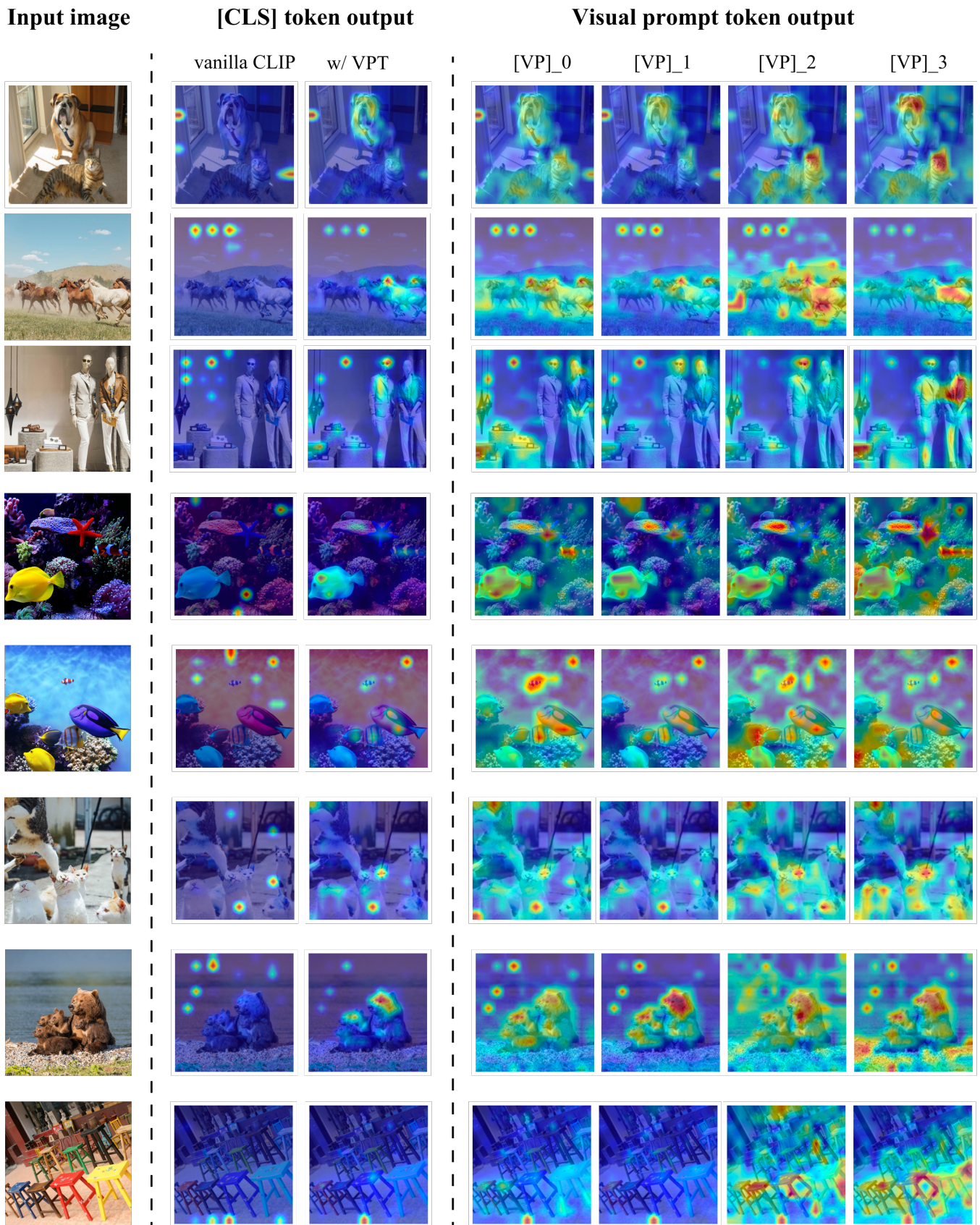


Figure 6: Attention maps of the class token ([CLS]) and the first four visual prompt tokens ([VP]s) to the patch tokens. The visual prompts are trained on ImageNet with 16-shot per category.